Post-processing methods of PIV instantaneous flow fields for unsteady flows in turbomachines

Cavazzini G.*, Dazin A. **, Pavesi G. *, Dupont P.**, Bois G. **,

** Department of Mechanical Engineering, University of Padova, Padova, Italy*
*** Laboratoire de Mécanique de LILLE (UMR CNRS 8107), Arts et Métiers ParisTech, École Centrale de Lille, France*

1. Introduction

Among the experimental techniques, the particle image velocimetry (PIV) is undoubtedly one of the most attractive modern methods to investigate the fluid flow in a non-intrusive way and allows to obtain instantaneous fluid flow fields by correlating at least two sequential exposures. This technique was successfully applied in several fields in order to study high complex three-dimensional flow velocity fields and to provide a significant experimental data base for the validation of combined numerical analysis models.

However, on one side, experimental limits and possible perturbing phenomena could negatively affect the PIV experimental accuracy, altering the real physics of the studied fluid flow field. On the other side, the huge amount of data obtainable by means of the PIV technique requires properly post-processing tools to be exploited in an in-depth study of the fluid-dynamical phenomena.

To avoid misinterpretation of the phenomena, complex cleaning techniques were developed and applied at the different steps of the PIV processing, starting from the acquired images (background subtraction, mask application, etc.) so as to increase the signal to noise ratio, and finishing to the instantaneous flow fields by means of statistical methods applied in order to identify residual spurious vectors [Raffel et al., 2002]. Even though all these methods allows to obtain a good filtering of the instantaneous flow fields, however they are not able to completely eliminate all the outliers in the results since the removal criteria are always dependent on the choice of a threshold value [Heinz et al., 2004; Westerweeel, 1994; Westerweel and Scarano, 2005].

To overcome this problem, the most common approach is to average the instantaneous PIV flow fields so as to improve the quality of the resulting flow field reconstruction and to more easily identify the flow field characteristics in the investigated area.

Several averaging methods were proposed and applied in literature. However their effectiveness in reducing the spurious vector number is strictly connected with the flow field characteristics, the experimental set-up and the acquisition characteristics of the PIV instrumentation.

The most simple but less accurate averaging procedure is undoubtedly the classical time average of a suitable number of instantaneous velocity fields, whose effectiveness is greatly affected by the quality of the starting velocity fields. To overcome the limits of this classical method still maintaining a similar approach, Meinhart et al. (2000) proposed to determine the time average of the instantaneous correlation functions so as determine with greater precision the correlation peak and hence the average velocity. Even though this method allow to increase the quality of the resulting averaged flow field, however it is not able to overcome the essential limit of the time-averaging methods, that is their inapplicability to unsteady flow fields and in particular to fluid-dynamical structures having a formation rate different from the framing rate of the camera. In addition to this, the method loses all the information about the evolution in time of the flow field, allowing to obtain only the averaged one.

To overcome these limits of the time-averaging methods and in particular their dependence from the framing rate of the camera, several phase-averaging methods were developed [Geveci et al. 2003; Perrin et al. 2007; Raffel et al. 1995, 1996; Schram and Riethmuller, 2001-2002; Ullum et al. 1997; Vogt et al. 1996; Yao and Pashal 1994]. These methods reorder and average the instantaneous flow fields on the basis of a proper phase, characterizing the development of the investigated phenomena so as to obtain a phase-averaged time series. These approaches, even though partially overcome the limits of the time-averaging methods, do not represent an universal solution to the problem of the data validation, since they require the characteristic frequencies of the phenomena to be known beforehand or to be determinable by combination with further experimental measurements (for example, pressure signals post-processed by spectral analysis). Moreover, they fail in case of not-periodical or frequency-combined structures, developing in the flow field.

In the first part of the chapter, a validation method of PIV results was proposed to critically analyse the quality and the meaningfulness of the experimental results in a PIV analysis on unsteady turbulent flow fields, commonly developing in turbomachines. The procedure was tested on the results of a classical phase-averaging method and was subdivided into three main steps: a convergence analysis to verify the fairness of the number of acquired images; an analysis of the probability density distribution to verify the repeatability of the velocity data; an evaluation of the maxima errors associated with the velocity averages to quantitatively analyse their trustworthiness. The procedure allowed to statistically verify the meaningfulness of the average flow field in unsteady flow conditions and to identify possible zones characterized by a low accuracy of the averaging method results.

In the second part of the chapter, a particular averaging method of PIV velocity fields was proposed to experimentally capture and visualize the unsteady flow field associated with an instability developing in a turbomachine with a known movement velocity. According to this method, the PIV flow fields was properly spatially moved according to its development velocity and was averaged on the basis of their new location. This procedure allowed to combine and average the flow fields in a frame moving with the instability so as to obtain a global visualization of the instability characteristics.

2. Validation method of PIV results

The experimental results, on which the validation procedure was tested, were obtained in a

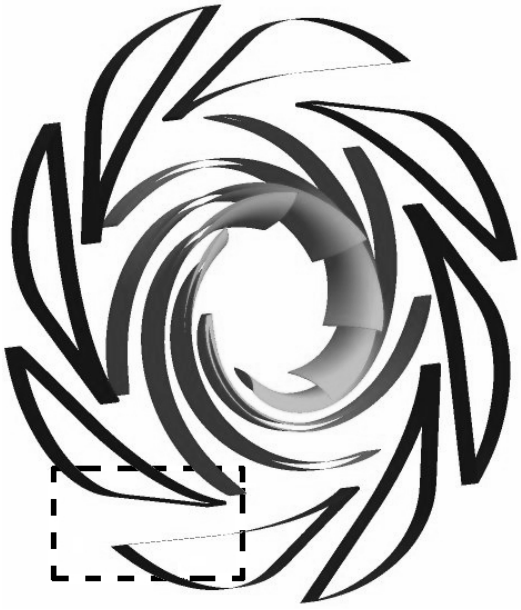

Figure 1 Schematic representation of the centrifugal pump. The dotted line indicates the investigated diffuser blade passage.

2D/2C PIV measurement campaign carried out on one diffuser blade passage of a centrifugal pump (fig. 1).

All the details about the test rig and the measurement devices, being outside the interest of this work, are not here reported, but can be found in previous studies [Wuibaut et al., 2001-2002].

As regards the images acquisition and processing, two single exposure frames were taken each two complete revolutions of the impeller and 400 instantaneous flow fields were determined for various operating conditions at different heights. A home-made software was used to treat and process the images so as to increase the signal to noise ratio (background subtraction, mask application, etc..) and a detailed cleaning procedure was applied to the instantaneous flow field to remove possible spurious vectors.

Since the turbulent phenomena under investigation were expected to be periodically associated with the impeller passage frequency, a phase-averaging technique based on this frequency was applied the instantaneous flow fields.

2.1 Convergence history

The first parameter to be considered to verify the meaningfulness of an averaged flow field is undoubtedly the number of acquired images, whose choice is generally affected by two conflicting aims. On one side, the meaningfulness of the averaged flow field that is favoured by a great number of acquired images; on the other side, the reduction of the acquisition time and of the required data storage capacity, increasing with the images number.

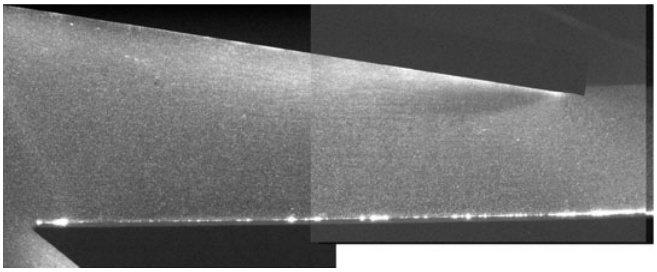

Figure 2 Seeding of the blade passage as seen by PIV cameras with an overlapping (black parts are the walls of the diffuser passage).

So, to determine a suitable number of images to be acquired, a convergence analysis, similar to that suggested by Wernert and Favier (1999), has to be applied.

This analysis studies the evolution in time of the average $\overline{C_N}(x,y)$ and of standard deviation $\varepsilon_N(x,y)$ of the absolute velocity C(x,y) over an increasing number of flow fields:

$$\overline{C_N}(x,y)=\frac{1}{N}\sum_{i=0}^{N}C(x,y,t_0+i\Delta t) \tag{1}$$

$$\varepsilon_N(x,y)=\sqrt{\frac{1}{N-1}\sum_{i=1}^{N}\left(\overline{C_i}(x,y)-\overline{C_{N\,max}}(x,y)\right)^2} \tag{2}$$

where N is the progressive number of flow fields (N=1,…N_{max}), N_{max} is the total number of determined flow fields, Δt is the sampling period, t_0 is the initial instant, $C(x,y,t_0+i\Delta t)$ is the absolute velocity at the coordinates (x, y) of the flow field (i+1), $\overline{C_i}(x,y)$ is the average of the absolute velocity determined over 'i' flow fields at the coordinates (x, y) and $\overline{C_{N\,max}}(x,y)$ is the average of the absolute velocity over the total number of acquired flow fields at the coordinates (x, y).

The analysis of the evolution in time of the average velocity and of its standard deviation allows to verify the existence of a minimum number of flow fields to be averaged so as to obtain a meaningful averaged flow field. For example, the convergence history of fig. 3 is

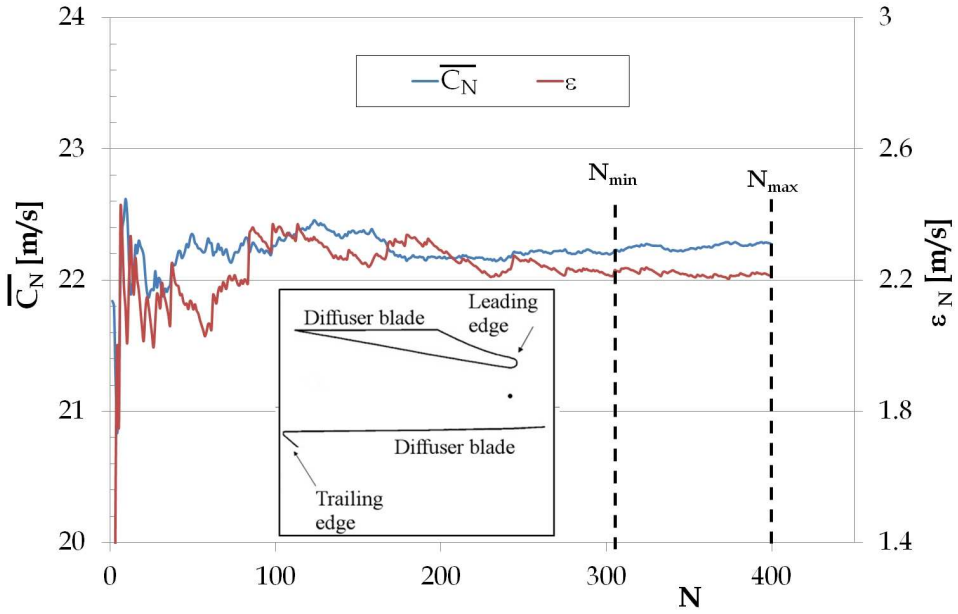

Figure 3 Convergence history in a point located at the entrance of the diffuser passage at mid-span.

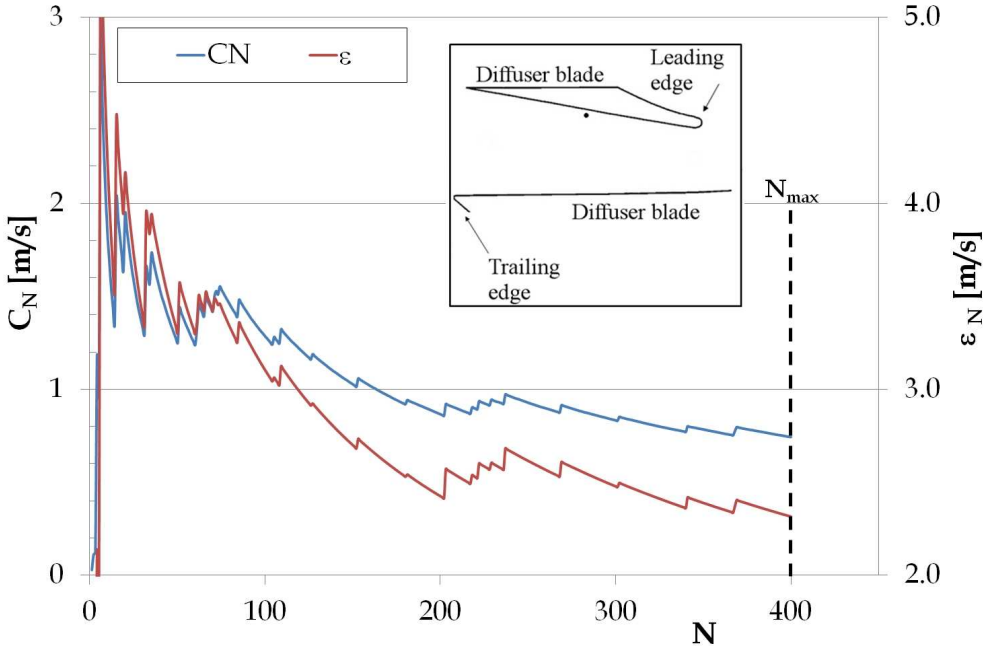

Figure 4 Convergence history in a point located in the middle of the diffuser passage at mid-span near the blade pressure side.

characterized by an asymptotic behaviour of the average and standard deviation with a asymptotic value reached after about 300 flow fields. This number represents the minimum number of flow fields to be determined in order to obtain a meaningful result. A greater number would not change the resulting average velocity and would not increase its meaningfulness.

A different behaviour characterized the convergence history of fig. 4, where both the average velocity and its standard deviation are not clearly stabilized after 400 flow fields. The velocity tends to zero and the standard deviation is of the order of the average velocity, highlighting a great perturbation of the instantaneous velocity values around the average one.

Before indistinctly increasing the number of images to be acquired, a critical analysis of the convergence history is necessary so as to consider the reasons of the non-convergent trend. The development of turbulence flows or unsteady structures in the zone of the reference point and/or experimental problems such as laser reflections or seeding problems should be considered. In fig. 4, as the reference point is located near the pressure side of the pump diffuser blade, laser reflection problems as well as spurious vectors owing to the boundary-layer development could not be excluded. The trend to zero of the progressive averaged velocity and the great values of the standard deviation support this hypothesis. In this case, the acquisition of a higher number of images would not probably guarantee the achievement of a meaningful averaged velocity value.

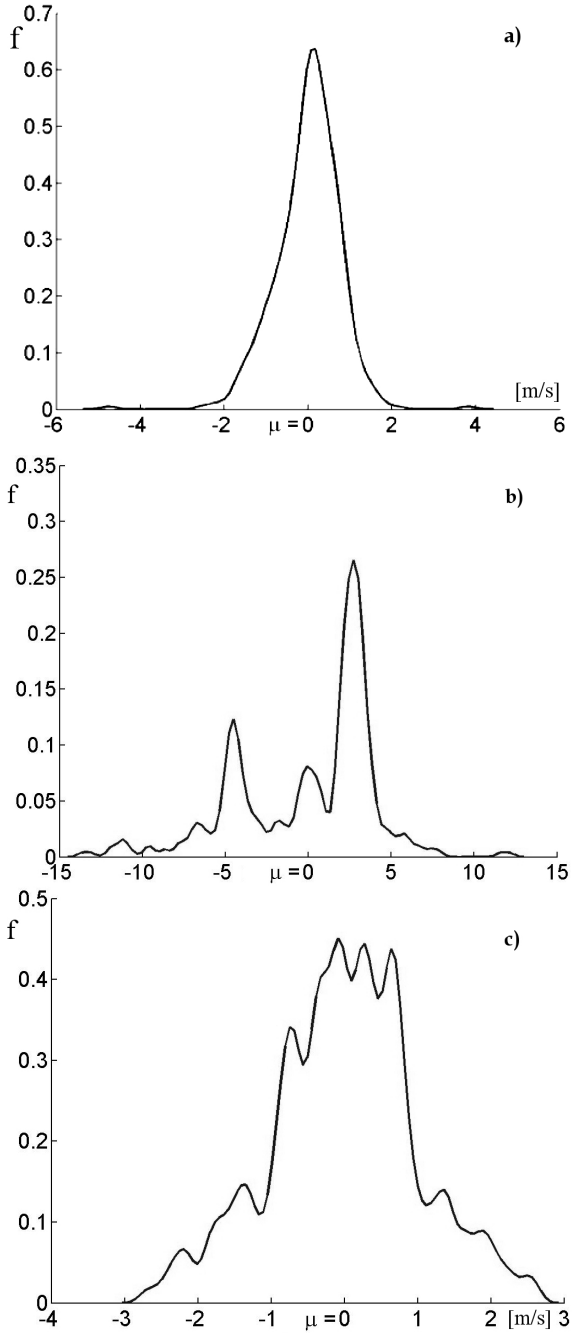

Figure 5 Examples of probability density distributions of velocity values

Hence, the convergence analysis appears to provide useful information about the proper choice of the number of images to be acquired, but allows only preliminary hypotheses on the quality of the results.

2.2 Probability density distribution

A phase-averaging method is based on the hypothesis that the experimental values to be averaged are repeated measures of the same experimental quantity. However, the repeatability of the experimental measurements in an investigated area could be invalidated by the possible development of non-periodical fluid-dynamical phenomena and by possible experimental problems. The lack of this repeatability, negatively affecting the accuracy of the phase-averaging method, is highlighted by a non-Gaussian probability density distribution of the experimental values. Therefore, the second step of the validation procedure is the analysis of the probability density distribution of the determined velocity values.

Since the aim of the analysis was to verify the Gaussianity of this distribution, no hypothesis on its form can be done. Hence, the probability density function has to be estimated using non-parametric kernel smoothing methods, with no hypothesis on the original distribution of the data [Bowman and Azzalini, 1997].

Figure 5 reports three examples of possible probability density distributions of velocity values,

translated to have zero mean value. In fig. 5a, the classical symmetric bell-shape of the Gaussian distribution testify the repeatability of the corresponding experimental measures. Moreover, the great values of the probability density function demonstrates the meaningfulness of the determined average velocity. In contrast, fig. 5b shows an asymmetric distribution of the data with multiple maxima and a wide dispersion of the values. In this case, the velocity average, corresponding to the abscissa $\mu = 0$, cannot be considered as meaningful, even if a higher number of images will be acquired, as the repeatability of the measures is not guaranteed.

The analysis of the probability density distribution could also allow to identify possible experimental problems. Indented bell-shaped distribution, as that reported in fig. 5c, clearly indicates the presence of peak-locking problems in the images acquisition. The peak-locking does not affect the mean velocity flow field but only its fluctuating part [Christensen, 2004] and is attributable to both the choice of the sub-pixel estimator and the under-resolved optical sampling of the particle images. So, even though this problem does not affect the meaningfulness of the average velocity value, its identification during a preliminary study could allow to correct the test rig set-up and to increase the quality of the instantaneous flow fields.

Even though the subjective visual analysis of the probability density distributions allowed a preliminary analysis of the measurement repeatability and of the presence of possible experimental problems, to effectively verify the normality of the velocity data distributions in the investigated area, it is necessary to apply a goodness-of-fit test. This test allows to verify the acceptance of the so-called 'null' hypothesis (i.e. if the data follow a specific theoretical distribution) or of the alternative hypothesis (i.e. if the data do not follow the specified distribution). The null hypothesis is rejected with a confidence level α, if the test statistic is greater than a critical value fixed at that confidence level. The greater the difference between the statistic and the critical value is, the greater the probability that the data do not follow the specified distribution.

In literature, several tests with different characteristics and powers are available (Pearson $\chi 2$, Anderson–Darling, Kolmogorov, Cramer–von Mises–Smirnov, and so on). The hypotheses of these tests can be divided into simple ones, when the parameters of the theoretical distribution to be checked are known, and complex ones, when the parameters of the theoretical distribution are determined using the same data sample to be tested. Complex hypotheses are typical of a PIV experimental analysis since the average μ and the standard deviation ε of the theoretical distribution are generally unknown and the average $\overline{C_N}(x,y)$ and the standard deviation $\varepsilon_N(x,y)$ of the sample are used as distribution parameters.

Among the available goodness-of-fit tests, the choice of the most proper one depends on the sampling conditions of the data. Lemeshko et al. (2007) compared the power of several goodness-of-fit tests by means of statistical modelling methods and based the choice on the desired confidence level and on the range of number of samples. For example, for 400 velocity values, as those of the experimental analysis considered as test case, and for a confidence level of 0.05 (5 per cent), the suggested goodness-of-fit test is the Anderson–Darling test.

However, the sampling conditions of an experimental analysis cannot be generalized in ranges and hence the trustworthiness of a goodness-of-fit test must be properly verified with a dedicated simulation. To do this, the test must be applied several times on random Gaussian samples having the same number of values of the experimental sample. The number of test applications has to be great enough to avoid of the simulation results on it. As this test is not time-expensive, the choice of a very high number of applications, such as 100 000, guarantees its negligible influence on the simulation results.

The trustworthiness of the goodness-of-fit test is verified once the error percentage of its application on Gaussian samples is lower or at most equal to the desired confidence level. In the example considered earlier, the Anderson–Darling test was applied 100 000 times on random Gaussian samples of 400 data, giving an error value of 5 per cent, which is not greater than the desired confidence level. This result demonstrates the applicability of the Anderson–Darling test to the experimental analysis sampling conditions.

Once verified its trustworthiness, the goodness-of-fit test has to be applied to each point of the investigated area so as to obtain a global visualization of the non-Gaussian critical zones of the flow field. Figure 6 reports an example of the Anderson-Darling application to the velocity flow fields determined in the diffuser passage. Cores of non-Gaussian distribution can be clearly identified at the entrance of the diffuser passage, near the blade walls and also in the mean flow (light grey circles in fig. 6). Even though it is always quite difficult to discriminate between fluid-dynamical and experimental problems, these results allow some preliminary hypothesis about the origin of these critical areas. At the diffuser entrance, the position of the impeller blade close to diffuser blade leading edge lets suppose the development of non-periodical turbulent phenomena coming from the impeller discharge,

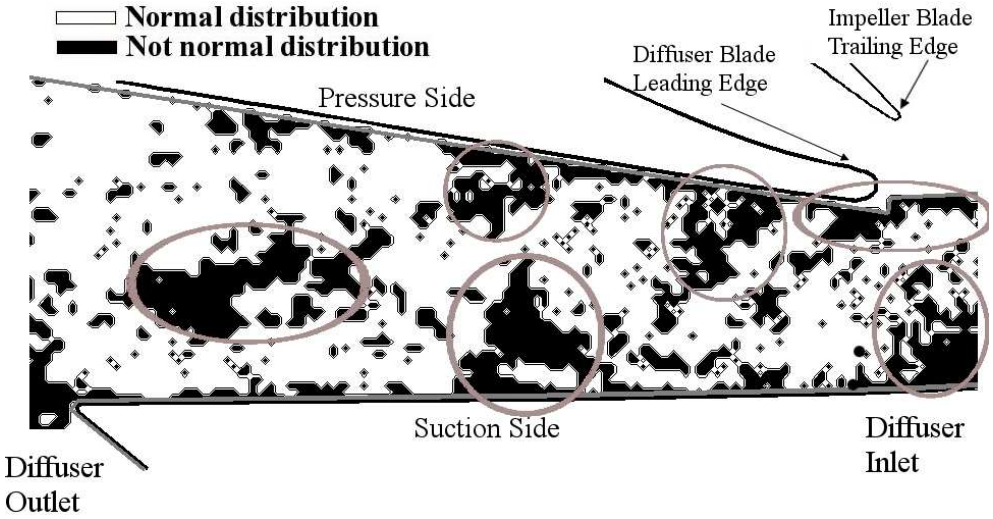

Figure 6 Example of the results of the Anderson-Darling test applied to the pump diffuser blade passage (the black line represents the blade profile; the dark grey line represents the limit of the mask applied to the grid and the light grey circles are marks to identify the non-Gaussian zones in the figure)

such as impeller blade wakes and/or rotor-stator interaction phenomena.

The non-Gaussian cores near the blade sides could be due to possible laser reflections problems or seeding problems, whereas laser reflections can be excluded for the cores in the mean flow because of their distance from the walls. These cores could be probably due to non-periodical phenomena proceeding in the passage, but this hypothesis has to be verified by numerical analysis of the flow field.

2.3 Confidence interval of the measured values

The validation procedure of the experimental results is completed by a measure of the reliability of the averaged flow field, that is obtained by estimation of the confidence interval of the determined averaged velocities, that depends on the effective distribution of the experimental data.

In the hypothesis of normal distribution, the confidence interval of the average velocity $\overline{C_N}(x,y)$ for a confidence level (1-α) is:

$$\left[\overline{C_N} - \frac{\varepsilon_N}{\sqrt{N}}\Phi^{-1}\left(1-\frac{\alpha}{2}\right), \overline{C_N} + \frac{\varepsilon_N}{\sqrt{N}}\Phi^{-1}\left(1-\frac{\alpha}{2}\right)\right] \tag{3}$$

where Φ is the normal cumulative distribution function and ε_N the standard deviation of the average velocity (Montgomery and Runger, 2003). So, in this hypothesis, the maximum error in the estimation of the average velocity is:

$$\frac{\varepsilon_N}{\sqrt{N}}\Phi^{-1}\left(1-\frac{\alpha}{2}\right) \tag{4}$$

When the goodness-of-fit test highlights not-normal distributions of the velocity values, to correctly determine the corresponding confidence interval, the effective distribution of the experimental data should be investigated. However, according to the central limit theorem, the procedure for estimating the confidence interval of normal samples can be also applied, with approximation, to not-normal samples if their dimension is sufficiently great (Montgomery and Runger, 2003). This estimation, even approximate, is useful to critically analysis the meaningfulness of the experimental results and to identify the problematic zones of the investigated area.

Figure 7 reports the distribution of the maxima errors (eq. (4)) that can be made in the evaluation of the averaged velocity in the diffuser blade passage. As it can be seen, the maxima errors are localized near the diffuser blade profiles in the inlet throat of the diffuser passage and could be attributed to the combination of the boundary-layer development with experimental problems such as reflection or seeding problems and to vortical cores coming from the impeller discharge on the suction side.

The further proof of the possible development of unsteady phenomena could be obtained by the spectral analysis of the velocity signals. Figure 8 reports the fast Fourier transform (FFT)

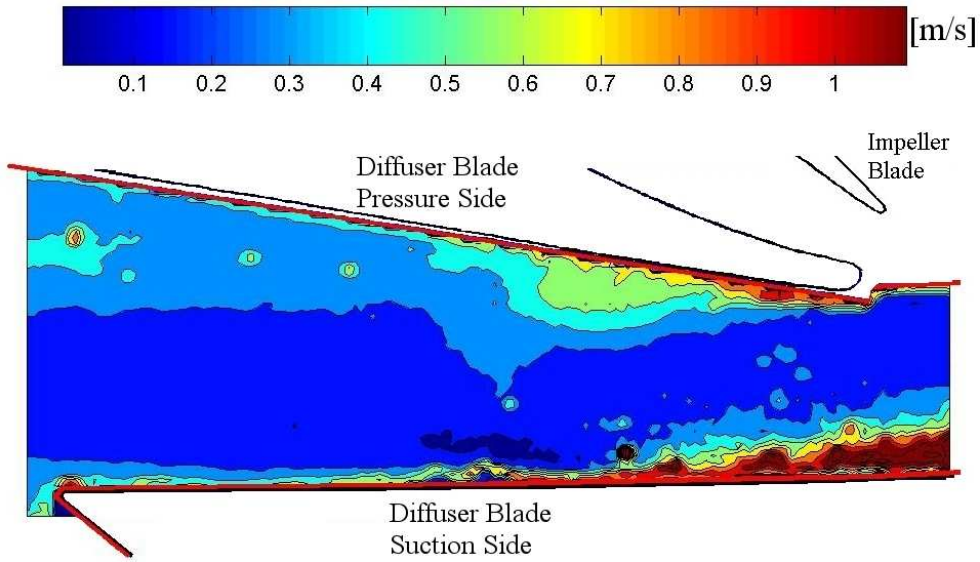

Figure 7 Example of distribution of the maxima errors of the averaged velocity in the diffuser passage (the black line represents the blade profile; the red lines represents the limit of the mask applied to the grid)

of the velocity components signals determined in three significant points of the flow field of fig. 7: near the suction side at the entrance of the diffuser passage (blue line), near the pressure side in the zone of maximum error (red line) and in the second half of the diffuser passage far from the blade profiles (black line). The FFT results are reported as a function of the ratio between the frequency f and the sampling frequency f_s of the data.

Concerning the velocity component in the mean flow direction Cx (fig. 8a), the points near the blade profiles (points 1 and 2) present peaks having amplitudes much greater than those of the point placed in the mean flow, whereas the velocity component in the direction normal to the mean flow Cy presents low FFT peaks for all the three points (fig. 8b). This strengthens the hypothesis of intense unsteady velocity fluctuations near blade profiles, proceeding in the mean flow direction, and hence confirms the results of the previous statistical analysis.

2.4 Comparison between experimental and numerical results: a critical validation

In fluid-dynamical investigations, the experimental results generally represent a significant reference database for the validation of combined numerical analysis models. However, since the experimental analysis could be negatively affected by experimental problems or post-processing limits, the possible discrepancies between experimental and numerical results have to be critically analysis in order to correctly identify the real error sources.

Numerical error sources, such as the grid resolution and the choice of the turbulent model, have to be considered in the comparison, but may not be the only causes. Experimental problems due to the test-rig or to unsteady phenomena could be also possible reasons for

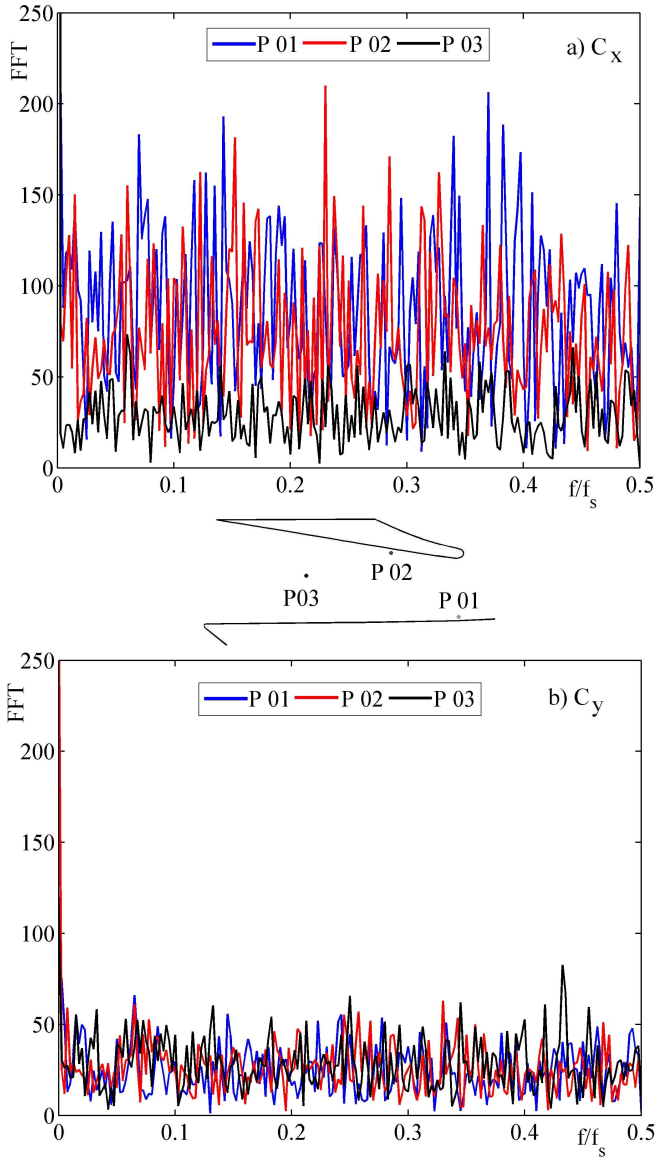

Figure 8 FFT of the velocity components signals determined in three points of the diffuser passage: at the entrance near the suction side (blue line), near the blade pressure side (red line) and in the second half of the diffuser passage far from the blade profiles (black line). a) Cx b) Cy

reflection problems or difficult seeding near the blades.

discrepancies. In this context, the validation procedure is extremely useful since it allows to identify the problematic zones of the investigated flow field and to appreciate the meaningfulness of the velocity averages for a critical comparison between the numerical and experimental results.

Figure 9 shows a comparison between the experimental results of fig. 7 and the results of a numerical analysis carried out on the same machine at the same operating conditions. Averaged velocity profiles determined in some sections of the diffuser blade passage are compared. The agreement is quite good, but there are some discrepancies near the diffuser blades (y/l=0 and y/l=1). Numerical error sources, such as a low stream-wise grid resolution or an improper choice of the turbulent model have to be considered as possible causes. However, the validation procedure previously applied to the PIV flow fields highlighted a low trustworthiness of the experimental averaged flow field near the blade profiles (fig. 7), indicating that the discrepancies between numerical and experimental results can be also due to experimental limits, such as

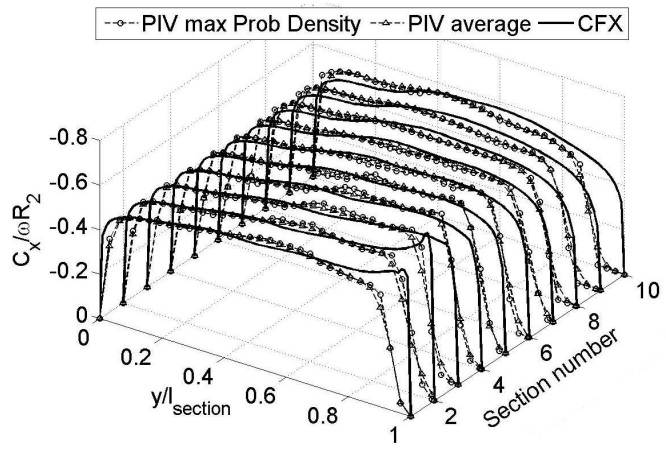

Figure 9 Comparison between experimental and numerical results: average velocity profiles in some sections of the diffuser passage

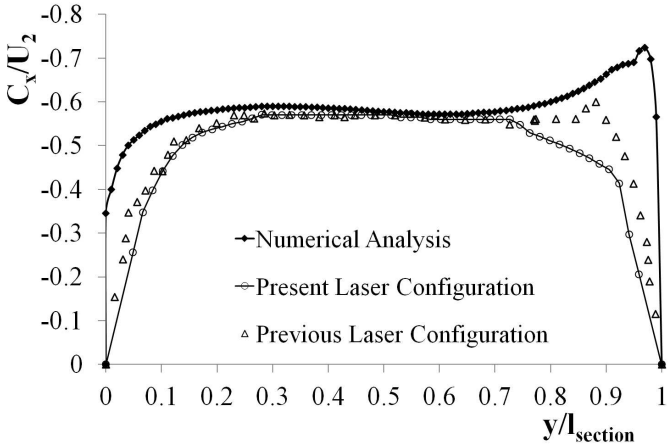

Figure 10 Effects of the modification of the laser sheet direction on the experimental results quality

In a preliminary study, this combined analysis could be also exploited to modify the set-up of the test rig so as to increase the experimental results quality in the problematic zones. For example, the possible reflection problems near the blade profiles of fig. 9 could be reduced modifying the laser configuration (fig. 10).

3. A new averaging procedure for instabilities visualization

PIV is now a method widely used in the field of Turbomachinery. It has proved its ability to provide useful experimental data for various research topics: rotor stator interaction in radial pumps or fans [Cavazzini et al., 2009; Meakhal & Park 2005; Wuibaut et al., 2002], tip-leakage vortex in axial flow compressors [Voges et al., 2011, Yu & Liu, 2007], swirling flow in hydraulic turbines [Tridon et al., 2010]. Nevertheless, in most cases, PIV was efficiently applied to catch phenomena which were correlated with the impeller rotation: PIV images were taken phase locked with the rotor. Consequently, with this kind of acquisition technique, the measurements were not able to treat phenomena, such as rotating stall or surge, whose frequencies are not constant or simply not linked with the impeller speed.

The recent development of high speed PIV offers new perspective for the application of the PIV technique in Turbomachinery. Van den Braembussche et al. (2010) have recently proposed a original experiment in which the PIV acquisition system was rotating with a

simplified rotating machinery. However, this technique does not overcome the problem of studying rotating phenomena whose frequency was not determined before the experiment.

To catch such type of phenomena, an original averaging procedure of the data based on a frequency or time-frequency analysis of a signal characteristic of the phenomenon was developed. The procedure was applied on two different test cases presented below: a constant rotating phenomenon and an intermittent one.

3.1 Experimental set-up of the test cases

The experimental results presented above were obtained in a PIV experimental analysis carried out on the so-called SHF impeller (fig. 11) coupled with a vaneless diffuser. The tests were made in air with a test rig developed for studying the rotor-stator interaction phenomena (fig. 12).

Figure 11 SHF impeller

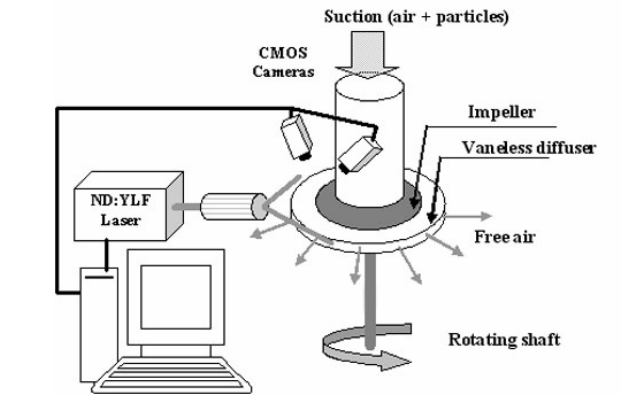

Figure 12 Experimental set-up

A 2D/3C High Speed PIV combined with pressure transducers was used to study the flow field inside the vaneless diffuser at several flow rates and at three different heights in the hub to shroud direction (0.25, 0.5 and 0.75 of the diffuser width) with an impeller rotation speed of 1200 rpm.

The laser illumination system consists of two independent Nd:YLF laser cavities, each of them producing about 20 mJ per pulse at a pulse frequency of 980 Hz.

Two CMOS cameras (1680 x 930 pixel^2), equipped with 50 mm lenses, were properly synchronized with the laser pulses. They were located at a distance of 480 mm from the measurement regions with an angle between the object plane and the image plane of about 45°.

All the details about the experimental set-up, being

outside the interest of this work, are not here reported, but can be found in a previous paper [Dazin et al., 2011].

The image treatment was performed by a software developed by the Laboratoire de Mecanique de Lille. The cross-correlation technique was applied to the image pairs with a correlation window size of 32 x 32 pixels^2 and an overlapping of 50%, obtaining flow fields of 80 x 120mm^2 and 81 x 125 velocity vectors. The correlation peaks were fitted with a three points Gaussian model. Concerning the stereoscopic reconstruction, the method first proposed by Soloff et al. (1997) was used. A velocity map spanned nearly all the diffuser extension in the radial direction, whereas in the tangential one was covering an angular portion of about 14°.

Each PIV measurement campaign was carried out for a time period of 1.6 seconds, corresponding to 32 impeller revolutions at a rotation speed of 1200 rpm. Since the temporal resolution of the acquisition was of 980 velocity maps per second, the time period of 1.6 second allowed obtaining 1568 consecutives velocity maps, corresponding to about 49 velocity maps per impeller revolution.

As regards the pressure measurements, two Brüel & Kjaer condenser microphones (Type 4135) were placed flush with the diffuser shroud wall at the same radial position (1.05 of diffuser inlet radius r_3) but at different angular position ($\Delta\theta$=75°). The unsteady pressure measurements, acquired with a sampling frequency of 2048 Hz, were properly synchronized with the PIV image acquisition system.

3.2 Constant angular velocity phenomena

At partial load and in particular at 0.26 Q_{des}, previous analyses showed that a rotating instability developed in the vaneless diffuser [Dazin et al., 2008]. The instability resulted to have a fundamental frequency equal to 0.84 of the impeller passage frequency and to be composed by three cells rotating around the impeller discharge with an angular velocity equal to 28% of the impeller rotation velocity ω_{imp} [Dazin et al., 2008].

The identification and visualization of the topology of these instability cells was not immediate since the angular span of one PIV map (about 14° of the whole diffuser) was much smaller than the size of an instability cell (about 75°).

To overcome this limit, a new averaging method was developed so as to combine the PIV velocity maps on the basis of the determined instability precession velocity and to obtain an averaged flow field in a reference frame rotating with the instability.

The knowledge of the instability angular speed was needed to be able to apply this procedure. This was determined through the analysis the crosspower spectrum of the pressure signals of the two microphones (Dazin et al 2008, 2011). This one was plotted and compared to the one obtained at design flow rate in Fig 13.
The spectrum at design flow rate was clearly dominated by the blade passage frequency f_b ($7 \cdot f_{imp}$). The $Q=0.26Q_{des}$ frequency spectrum was overcome by several peaks in the frequency band between 0.5fimp and 2.0fimp, particularly by the frequency $f_{ri} = f/f_{imp}=0.84$, that was demonstrated, (Dazin et al 2008), to be the fundamental frequency of a rotating instability composed by three cells rotating around the impeller discharge with an angular velocity equal to 28% of the impeller rotation velocity.

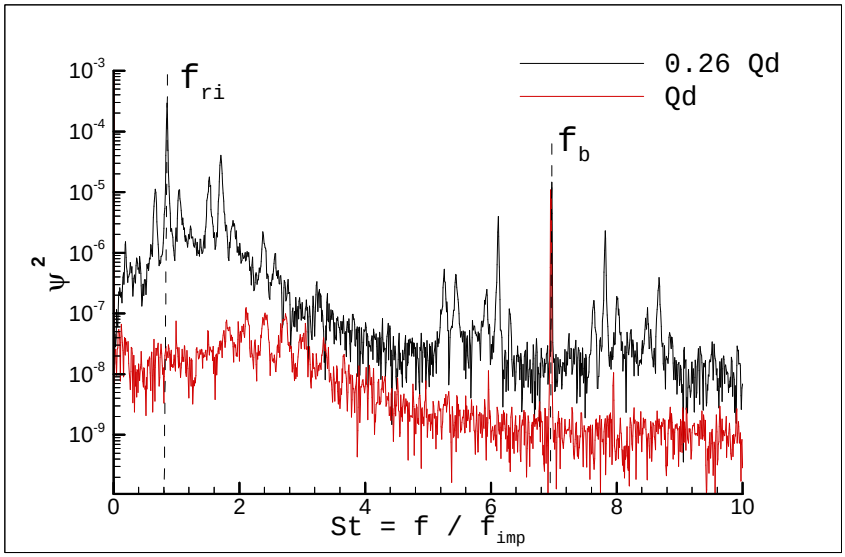

Fig 13 Crosspower spectra of pressure signals

Then the PIV averaging procedure could have been applied: first ,Since the measurements were not synchronized with the instability rotation, the velocity maps could not be exactly superimposed at each impeller revolution. So it was necessary to create a mesh (Fig 14), having the same dimensions of the diffuser ($0<\theta<360°$, $0.257<r<0.390$ m), to be used as reference grid for the combination of the PIV maps. To have an almost direct correspondence between this mesh and the PIV grid, the size of one cell of the mesh was fixed roughly equal to the size of one cell of the PIV grid. Then, the first velocity map was bi-linearly interpolated on the new grid, as shown for the tangential velocities in fig. 15a. The velocity values of the mesh were fixed equal to zero (green in the figure) except in the zone corresponding to the first PIV map properly interpolated on the reference grid. Since the reference frame was fixed to rotate with the instability, the second velocity map was added in the new mesh after a rotation of an angle equal to the instability velocity multiplied by the sampling period of the PIV measurements. As this second velocity map overlapped the first one, in the overlapping zone the velocity values were properly averaged. This operation was repeated for the following velocity maps till a complete revolution of the instability, corresponding to 175 maps, was made. Afterwards, the maps were averaged with the ones of the previous revolution(s). Examples of the averaging computation results respectively after 10, 80 and 175 velocity maps are reported in fig. 15(b-d). At the end of the procedure, 120 velocity vectors were averaged in each point of the reference grid, obtaining a mean velocity vector. The standard deviation was of the order of 2 m/s and the corresponding 95% confidence interval for each averaged velocity component $\overline{c}_i$ was:

$$\left[\overline{c}_i \pm 0.4 m/s\right]$$

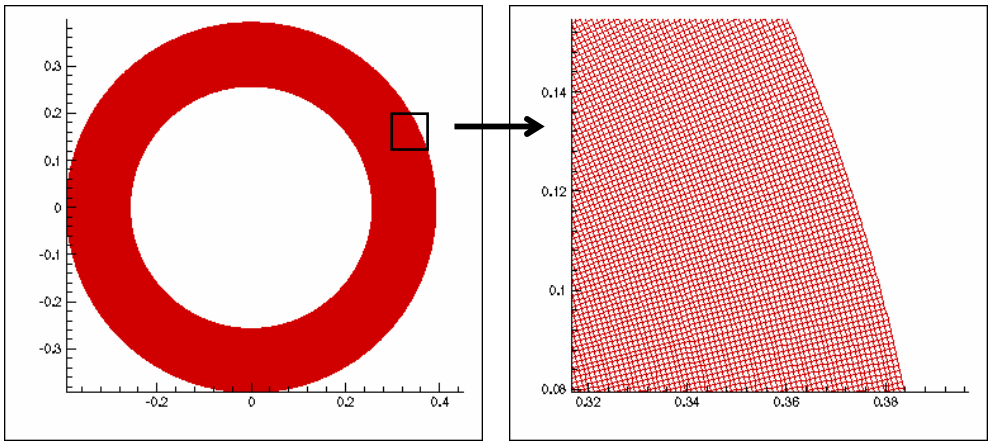

Figure 14 : Mesh used for the averaging procedure

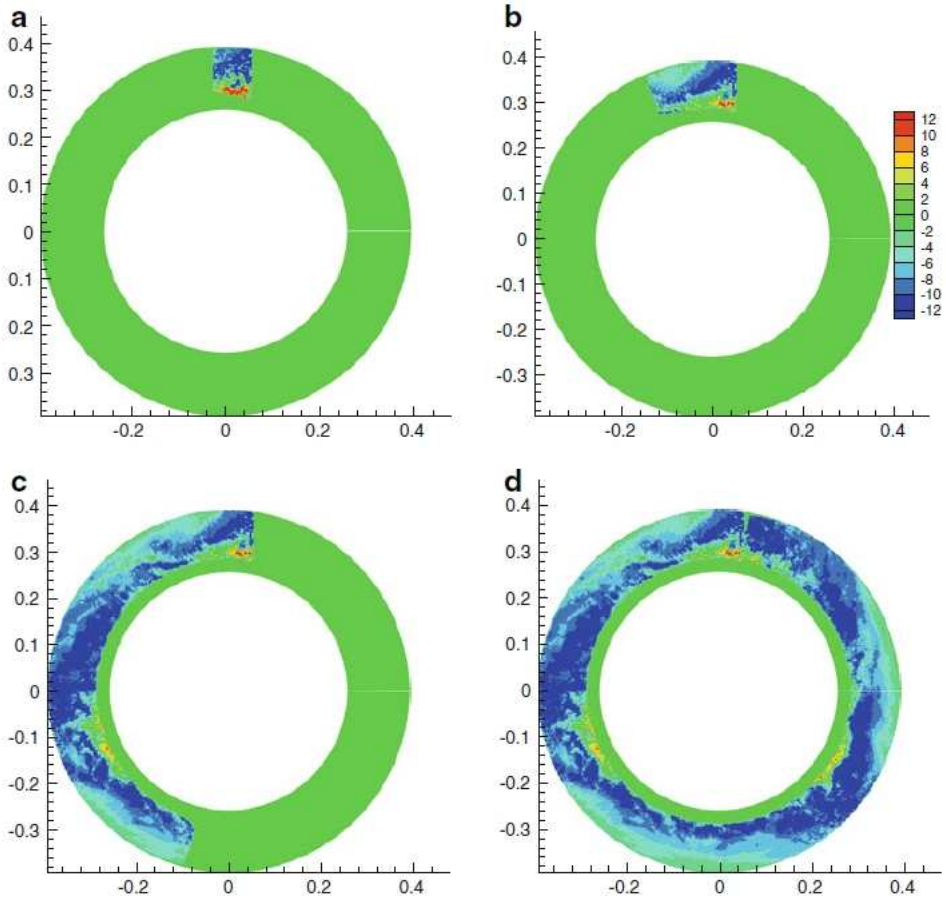

Figure 15 Averaging computation results after 1, 10, 80 and 175 velocity maps for the tangential velocity component at mid span (in m/s)

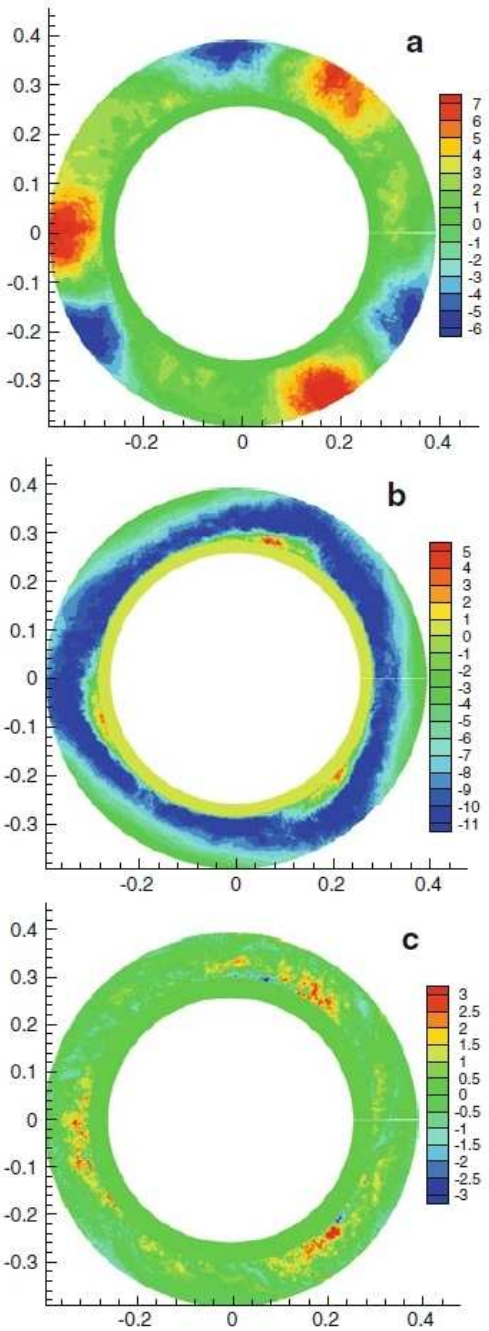

Figure 16 Results of the averaging procedure: a) radial velocity; b) tangential velocity; c) axial velocity [m/s]

The procedure described above allowed to obtain averaged flow fields in a reference frame rotating with the instability for the three velocity components (fig. 16). Because of laser sheet reflections on the impeller blades, several instantaneous flow fields were negatively affected at the diffuser inlet by the proximity of the impeller blades. For this reason, the averaged flow fields are presented only for r> 0.3 m. The average flow field of the radial velocity component shows three similar patterns composed of two cores, respectively of inward and outward radial velocities, located near the diffuser outlet (fig 16a).In correspondence to these two cores, a zone of negative tangential velocity is identifiable near the diffuser inlet (fig. 16b) and a zone of slightly positive axial velocity is outlined within the diffuser (fig 16c).

So, the averaging procedure allowed to clearly visualize the topology of the instability rotating in the diffuser and to obtain several information about its fluid-dynamical characteristics.

3.3 Intermittent phenomena

In the same pump configuration at a greater flow rate (0.45 Q_{des}), rotating instabilities were still identified in the diffuser, but resulted to be characterized by two competitive low-frequency modes.

The first mode, which dominated the spectrum, corresponded to an instability composed by two cells rotating at ω/ω_{imp} = 0.28, whereas the second mode corresponded to an instability composed by three cells rotating at ω/ω_{imp} = 0.26 [Pavesi et al., 2011]. Moreover, the time-frequency analysis, carried out on the pressure signals, highlighted that these two competitive modes did not exist at the same time but were present intermittently in the diffuser (fig. 17).

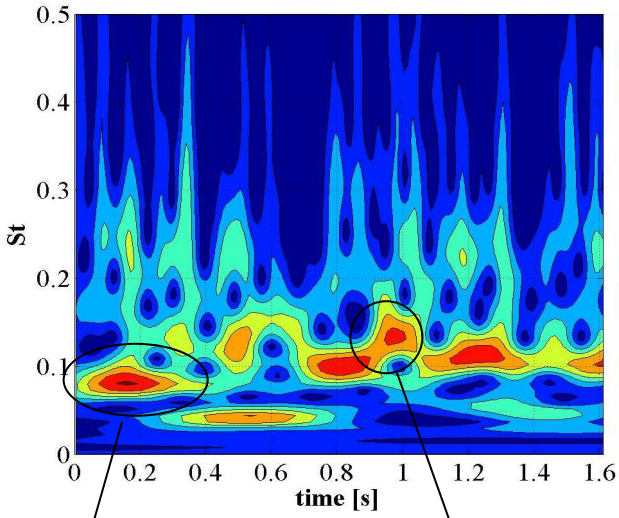

Figure 17 Detail of the wavelet analysis of the pressure signals acquired at Q/Q_{des} = 0.45

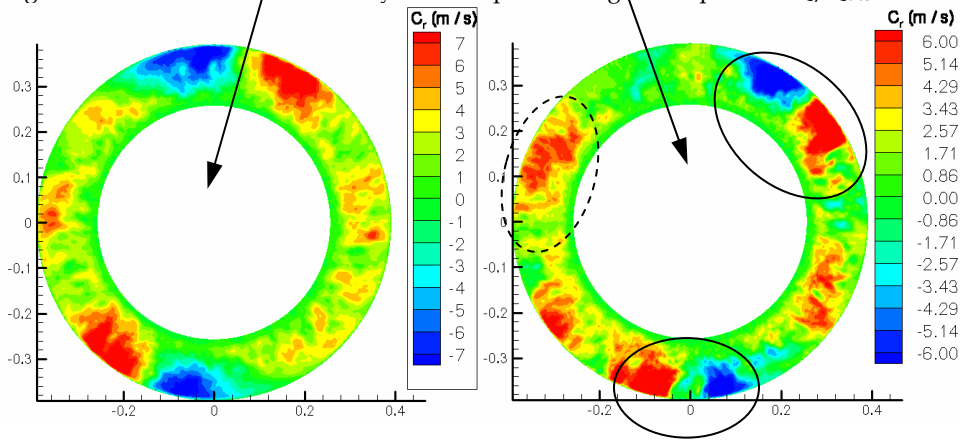

Figure 18 PIV averaging procedure results for the two modes identified at Q/Q_{des} = 0.45

Consequently, the averaging procedure defined in §3.2 could not be immediately applied to the PIV results but it was adapted to the new intermittent characteristics of the fluid-dynamical instability. In particular, the results of the time frequency analysis were used to determine the time periods of the acquisition process during which only one mode was dominant. Then, the PIV averaging procedure, described in §3.2, was applied only to the flow fields determined in those time periods characterized by the presence of one mode. In this way, two averaged flow fields corresponding to the two competitive modes were obtained (fig. 18).

For example, the first mode resulted to be dominant in a time period of about 0.4 s at the beginning of the simultaneous pressure and PIV acquisitions. Consistently with the Fourier spectra analysis, the PIV averaged velocity map (fig. 18a) obtained on this time period

presents two instability cells diametrically located, similar to those obtained at the lowest flow rate.

For the second mode, the longer time period identified was of only about 0.1 s. The averaged velocity procedure applied on this time period gives the velocity map plotted on fig 18b. For this mode, the expected number of cells was three, whereas the averaged velocity map presents only two clear cells (surrounded by a solid line). The third cell of this mode is hardly visible (inside the dashed lines), most probably because of a too-short period for the application of the PIV averaging procedure.

4. Conclusions

This work presents two different post-processing procedures suitable to be applied to PIV instantaneous flow fields characterized by the development of unsteady flows.

The first procedure was focused on the PIV experimental accuracy and was aimed at the validation of the averaged flow fields in a PIV analysis. This procedure combines several statistical tools and can be summarized in three main steps:

- a convergence analysis to verify that the number of acquired images allowed to obtain a meaningful averaged flow field
- the analysis of the probability density distribution to verify the repeatability of the measurements and to identify the critical area of the investigated flow field.
- the estimation of the confidence interval to evaluate the maxima errors associated with the determined velocity averages and hence to quantitatively analyze their trustworthiness.

This validation procedure can be considered not only as a necessary critical analysis of the meaningfulness of experimental PIV results, but also as a possible preliminary study for improving the test rig before starting time- and work-intensive measurement campaigns.

The second part of the chapter is focused on the averaging techniques and presents an original averaging procedure of PIV flow fields for the study of unforced unsteadiness. Since the spectral characteristics of the instability and in particular its precession velocity has to be known, the procedure is necessarily combined with a spectral analysis of simultaneously acquired pressure signals.

On the basis of the spectrally determined instability velocity, the PIV flow fields were properly combined and averaged, obtaining an average flow field in the reference frame of the instability to be studied. This result allows to capture and visualize the topology of the phenomenon and to obtain more in-depth information about its fluid-dynamical development and characteristics.

The procedure was also developed and adapted for intermittent instability configurations, characterized by competitive modes alternatively present in the flow field.

5. References

Bowman, A.W. & Azzalini, A. (1997). Applied smoothing techniques for data analysis: the kernel approach with S-plus illustrations, 1997, Oxford University Press, New York.

Cavazzini, G.; Pavesi, G.; Ardizzon, G.; Dupont, P.; Coudert, S.; Caignaert, G. & Bois, G. (2009). Analysis of the Rotor-Stator Interaction in a Radial Flow Pump. *La Houille Blanche, Revue Internationale de l'eau*, n. 5/2009, pp. 141-151.

Christensen, K. T. (2004). The influence of peak-locking errors on turbulence statistics computed from PIV ensembles. *Experiments in Fluids*, vol. 36, pp. 484-497.

Dazin, A.; Coudert, S.; Dupont, P.; Caignaert, G. & Bois, G. (2008). Rotating Instability in the Vaneless Diffuser of a Radial Flow Pump. *Journal of Thermal Science*, vol. 17(4), pp. 368-374.

Dazin, A.; Cavazzini, G.; Pavesi, G.; Dupont, P.; Coudert, S.; Ardizzon, G.; Caignaert, G. & Bois, G. (2011) High-speed stereoscopic PIV study of rotating instabilities in a radial vaneless diffuser. *Experiments in Fluids*, vol. 51 (1), pp. 83-93.

Geveci, M.; Oshkai, P.; Rockwell, D.; Lin, J.-C. & Pollack, M. (2003). Imaging of the self-excited oscillation of flow past a cavity during generation of a flow tone. *Journal of Fluid and Structures*, vol. 18, pp. 665-694

Heinz,O.; Ilyushin, B. & Markovic, D. (2004). Application of a PDF method for the statistical processing of experimental data. *International Journal of Heat and Fluid Flow*, Vol. 25, pp. 864–874.

Lemeshko, B. Y.; Lemeshko, S. B. & Postovalov, S. N. (2007). The power of goodness of fit tests for close alternatives. *Measurement techniques*, vol. 50(2), pp. 132-141.

Meakhail, T. & Park, S.O (2005). A Study of Impeller-Diffuser-Volute Interaction in a Centrifugal Fan, *Journal of Turbomachinery*, vol. 127(1), pp. 84-90.

Meinhart, C. D.; Werely, S. T. & Santiago, J. G. (2000). A PIV algorithm for estimating time-averaged velocity fields. *Journal of Fluids Engineering*, Vol. 122, pp. 285–28

Montgomery, D. C. & Runger, G. C. (2003). Applied statistics and probability for engineers, 2003, John Wiley & Sons, NewYork.

Pavesi, G.; Dazin, A.; Cavazzini, G.; Caignaert, G.; Bois, G. & Ardizzon, G. (2011). Experimental and numerical investigation of unforced unsteadiness in a vaneless radial diffuser. *ETC 9, 9th Conference on Turbomachinery, Fluid Dynamics and Thermodynamics*, Istanbul (Turkey), March 21-25, 2011

Perrin, R.; Cid, E.; Cazin, S.; Sevrain, A.; Braza, M.; Moradei, F. & Harran, G. (2007). Phase-averaged measurements of the turbulence properties in the near wake of a circular cylinder at high Reynolds number by 2C-PIV and 3C-PIV. *Experiments in Fluids*, Vol. 42, pp. 93–109.

Raffel, M.; Kompenhans, J. & Wernert, P. (1995). Investigation of the unsteady flow velocity field above a airfoil pitching under deep dynamic stall conditions. *Experiments in Fluids*, Vol. 19, pp. 103–111.

Raffel, M.; Seelhorst, U.; Willert, C.; Vollmers, H.; Bütefisch, K. A. & Kompenhans, J. (1996). Measurements of vortical structures on a helicopter rotor model in a wind tunnel by LDV and PIV, *Proceedings of the 8th International Symposium on Applications of laser techniques to fluid mechanics*, pp. 14.3.1–14.3.6, Lisbon, Portugal, 1996.

Raffel, M.; Willert, C.; Werely, S. & Kompenhans, J. (2002). Particle image velocimetry – a practical guide, 2007, Springer-Verlag, Berlin.

Schram, C. & Riethmuller, M. L. (2001). Evolution of vortex ring characteristics during pairing in an acoustically excited jet using stroboscopic particle image velocimetry, *Proceedings of the 4th International Symposium on Particle image velocimetry*, paper 1157, Gottingen, Germany, September 17–19, 2001.

Schram, C. & Riethmuller, M. L. (2002). Measurement of vortex ring characteristics during pairing in a forced subsonic air jet. *Experiments in Fluids*, Vol. 33, pp. 879–888.

Soloff, S.M.; Adrian, R.J. & Liu, Z.C. (1997). Distortion compensation for generalized stereoscopic particle image velocimetry. *Measurement Science and Technology*, vol. 8, pp. 1441-1454.

Tridon, T.; Stéphane, B.; Dan Ciocan, G. & Tomas, L. (2010). Experimental analysis of the swirling flow in a Francis turbine draft tube: Focus on radial velocity component determination. *European Journal of Mechanics - B/Fluids*, vol. 29(4), July-August 2010, pp. 321-335

Ullum, U.; Schmidt, J.J.; Larsen, P.S. & McCluskey, D.R. (1997). Temporal evolution of the perturbed and unperturbed flow behind a fence: PIV analysis and comparison with LDAdata, *Proceedings of the 7th International Conference on Laser anemometry and applications*, pp. 809–816, Karlsruhe, Germany, 1997.

Van den Braembussche, R.A.; Prinsier, J. & Di Sante, A. (2010). Experimental and Numerical Investigation of the Flow in Rotating Diverging Channels. *Journal of Thermal Science*, Vol. 19 (2), pp. 115−119

Voges, M.; Willert, C.; Mönig, R.; Müller, M.W & Schiffer, H.P. (2011). The challenge of stereo PIV measurements in the tip gap of a transonic compressor rotor with casing treatment. *Experiments in Fluids,* DOI 10.1007/s00348-011-1061-y

Vogt, A.; Baumann, P.; Gharib, M. & Kompenhans, J. (1996). Investigations of a wing tip vortex in air by means of DPIV. *AIAA* Paper 96-2254

Wernert, P. & Favier, D. (1999). Considerations about the phase-averaging method with application to ELDV and PIV measurements over pitching airfoils, *Experiments in Fluids*, Vol. 27, pp. 473-483

Westerweel, J. (1994). Efficient detection of spurious vectors in particle image velocimetry data, *Experiments in Fluids,* vol. 16, pp. 236-247

Westerweel, J. & Scarano, F. (2005). Universal outlier detection for PIV data, *Experiments in Fluids*, vol. 39, pp. 1096-1100.

Wuibaut, G.; Dupont, P.; Bois, G.; Caignaert, G. & Stanislas, M. (2001). Analysis of flow velocities within the impeller and the vaneless diffuser of a radial flow pump. *Proc. IMechE, Part A: Journal of Power and Energy*, Vol. 215(A6), pp. 801–808, doi: 10.1243/0957650011538938.

Wuibaut, G.; Dupont, P.; Bois, G.; Caignaert, G. & Stanislas, M. (2002). PIV measurements in the impeller and the vaneless diffuser of a radial flow pump in design and off design operating conditions, *Journal of Fluid Engineering, Transactions ASME*, Vol. 124(3), pp. 791–797.

Yao, C. & Pashal, K. (1994). PIV measurements of airfoil wake-flow turbulence statistics and turbulent structures. *AIAA* Paper 94-0085

Yu, X.J. & Liu, B.-J. (2007). Stereoscopic PIV measurement of unsteady flows in an axial compressor stage. *Experimental Thermal and Fluid Science*, vol. 31, pp. 1049–1060